

Article

# Shock-Induced Olivine-Ringwoodite Transformation in the Shock Vein of Chondrite GRV053584

Feng Yin <sup>1,2</sup> , Zhiwei Liao <sup>3,4,\*</sup>, Andrew Hursthouse <sup>1,5</sup>  and Deqiu Dai <sup>2</sup>

<sup>1</sup> Hunan Provincial Key Laboratory of Shale Gas Resource Utilization, Hunan University of Science and Technology, Xiangtan 411201, China; fengite@hotmail.com (F.Y.); andrew.hursthouse@uws.ac.uk (A.H.)

<sup>2</sup> Department of Geology, Hunan University of Science and Technology, Xiangtan 411201, China; ddqygf@163.com

<sup>3</sup> College of Resources and Environmental Science, Chongqing University, Chongqing 400044, China

<sup>4</sup> State Key Laboratory of Coal Mine Disaster Dynamics and Control, Chongqing University, Chongqing 400044, China

<sup>5</sup> School of Science and Sport, University of the West of Scotland, Paisley PA1 2BE, UK

\* Correspondence: zwliao16@cqu.edu.cn; Tel.: +86-23-6510-5093

Received: 2 February 2018; Accepted: 30 March 2018; Published: 1 April 2018



**Abstract:** Shock metamorphism of minerals in meteorites could help to understand the shock history of its parent body and also provide a window into the interior of the Earth. Although shock features in olivine have been well known within and adjacent to shock melt veins and shock melt pockets in meteorites, there are processes that are not yet completely understood. Ringwoodite is formed by crystallization from olivine melts or solid-state phase transformation of olivine. Typically, olivine clasts with a ringwoodite rim around an olivine core have been documented from only a handful of meteorites. Here we report results from GRV053684, a highly shocked L6 chondrite that was collected by Chinese Antarctic Research Expedition in 2006 to Antarctica. The investigations of the shock pressure history and the transformation mechanism of olivine to ringwoodite use optical microscope, electron probe microanalyzer (backscattered electron images, major element quantitative analyses, and quantitative wavelength-dispersive spectrometry elemental X-ray maps), and Raman spectrograph. Ringwoodite in the shock melt vein generally displays as Fe-rich (Fa<sub>37-43</sub>) polycrystalline rims around Fe-poor (Fa<sub>11-20</sub>) olivine core and as small individual clasts embedded in shock melt vein matrix. The difference in FeO between ringwoodite rim and olivine core implies that Fe was preferentially partitioned to ringwoodite. The occurrence of maskelynite (An<sub>17</sub>) indicates a shock pressure ~30 GPa. The FeO and MgO diffusion indicates the transformation process of olivine to ringwoodite is a diffusion-controlled incoherent nucleation and growth. The spatial association between ringwoodite and the shock melt vein matrix suggests that high temperature plays a key role in prompting phase transformation.

**Keywords:** shock metamorphism; olivine; ringwoodite; phase transformation

## 1. Introduction

Shock metamorphism is one of the fundamental geological processes in the evolution of meteorites [1]. The parent body of meteorites undergoes one or more impact events in space, and the minerals in the meteorites are modified by shock-induced high pressures and high temperatures. Therefore, shock effects seen in these minerals are records of the shock conditions [2,3]. Understanding the processes involved in formation of these shock effects is fundamental for any interpretations of the impact events. Furthermore, shock-induced high pressures and high temperatures cover the pressures and temperatures condition of the Earth's mantle. Thus, shock effects in minerals can reveal the shock history of its parent body and are also a window into the processes in the interior of the Earth.

Olivine is a common rock-forming mineral that is widely distributed in ultramafic rocks, mafic rocks, and meteorites and its high pressure polymorphs are the most abundant minerals in the Earth's upper mantle [4,5]. The chemical formula of olivine is  $A_2SiO_4$ , where A is a mixed portion of  $Fe^{2+}$ ,  $Mg^{2+}$ ,  $Ni^{2+}$ ,  $Mn^{2+}$  and  $Ca^{2+}$ . Because of the hypervelocity impact on the parent body of the meteorite, olivine in the meteorites always has been modified by shock waves and they usually display shock metamorphic features, such as undulatory extinction, mosaicism, planar fractures, planar deformation features, phase transformation, melting, and decomposition [2,6–9]. Olivine provides an index for a meteorite shock classification scheme, i.e., shock levels of S1 (unshocked) to S6 (very strongly shocked) [3,10,11]. Wadsleyite and ringwoodite are high pressure phases of olivine. Under progressive high pressure and temperature, olivine transforms first into wadsleyite and then into ringwoodite. Seismic discontinuities in the upper mantle (410 km) and in the transition zone (~520 km) are attributed to olivine-wadsleyite transformation and wadsleyite-ringwoodite transformation, respectively [12]. Olivine might also transform to ringwoodite in the subducting lithosphere [13,14]. In the lower mantle (>660 km), ringwoodite decomposes to (Mg,Fe)SiO<sub>3</sub>-perovskite (named bridgmanite) and (Mg,Fe)O-periclase [15–20]. Natural ringwoodite was first discovered in the Tenham L6 chondrite [21], and so far it was identified only in shocked meteorites, such as ordinary chondrites, carbonaceous chondrites, lunar meteorites, and Martian meteorites [6,8,22–28], except one terrestrial sample, as an inclusion in a tiny diamond crystal [29]. Ringwoodites in meteorites are generally found within or directly adjacent to shock-melt veins and pockets, where it mainly occurs as fine grained polycrystalline aggregates [27,30] and lamellar [22,31]. Phase transformation is a complex process. The phase transformation of olivine-ringwoodite can be induced by an incoherent intercrystalline diffusion controlled mechanism [32,33] or an interface-controlled mechanism [34], a coherent intracrystalline martensitic transformation [35,36], a nucleation and growth mechanism [37], or an incoherent intracrystalline transformation [38,39].

This study focuses on the shock-metamorphic features of olivines in a single shock vein of chondrite GRV053584. We try to understand the shock history of GRV053584 and uncover the transformation mechanism of olivine to ringwoodite.

## 2. Sample and Methods

The GRV053584 was collected by the Chinese Antarctic Research Expedition in 2006 in the Antarctica region. Its total mass was 2.8 g, originally classified as an L6 chondrite (Figure 1). The specimen is held by the Polar Research Institute of China, from which one polished section was obtained through loan for this study.



**Figure 1.** An overview of the chondrite GRV053584. Each thick line grid is 1 cm.

Initial examination of the polished section with an optical microscope in reflected light confirmed that this meteorite was strongly affected by shock metamorphism, which caused small volumes of the rock to melt forming a shock vein. Several areas of interest within and surrounding the shock vein were selected for further detailed petrographic, mineralogical, and chemical characterization. Raman spectroscopy performed on minerals was obtained in the range of 100–1200  $\text{cm}^{-1}$  by a Renishaw RM-2000 instrument (Renishaw, Gloucestershire, UK) ( $\text{Ar}^+$  laser, 514 nm line, 0.7- $\mu\text{m}$ -wide spots) at the Guangzhou Institute of Geochemistry, Chinese Academy of Sciences (GIGCAS) with a 60 s acquisition time. Backscattered electron (BSE) imagery of samples and quantitative analyses of minerals (olivine, ringwoodite, plagioclase, maskelynite) was undergone using a JEOL JXA-8230 electron probe microanalyzer (EPMA) (JEOL, Tokyo, Japan) at the Key Laboratory of Mineralogy and Metallogeny in GIGCAS. The analyses were conducted with an acceleration voltage of 15 kV, a beam current of 20 nA, and a peak counting time of 20 s. The diameters of the analyzed spots were 10  $\mu\text{m}$  for maskelynite and 1  $\mu\text{m}$  for other minerals. The quantitative data obtained was in weight percentage of oxides (wt %). A set of standards (synthetic and natural minerals and oxides) from SPI Supplies, USA and from National Technical Committee for Standardization of Microbeam Analysis, China was used for routine calibration. Analytical results were reduced using the ZAF correction routines. The standards used were olivine for Si and Mg, magnetite for Fe, diopside for Ca, and Ni metal for Ni. Relative precisions are  $\pm 2\%$  for Si, Fe and Mg and  $\pm 5\%$  for Ca and Ni. For olivine and ringwoodite, Fe contents are expressed as a fayalite equivalents, computed as  $(100 \text{ Fe}/[\text{Fe} + \text{Mg}])$  on a molar basis. The X-ray mapping was carried out using the same JEOL JXA-8230 electron microprobe as the major element quantitative analyses at the GIGCAS. The operation conditions of an accelerate voltage of 20 kV, a probe current of 300 nA and a beam size of 1–4  $\mu\text{m}$  were adopted for mapping. Mg was analyzed using a TAP crystal and Fe was analyzed using an LIF crystal.

### 3. Results

#### 3.1. Shock Vein in the GRV053584

There is only one large shock vein with a width of 20–1000  $\mu\text{m}$  in the GRV053584 (Figure 2). The shock vein cuts across the chondritic host rock and is located along the sample boundary. Boundaries between the chondritic portion and the shock vein are clear and smooth. The shock vein consists of a number of mineral fragments, lithic clasts, and 30%–40% fine-grained matrix. The coarse-grained lithic clasts are chondritic xenoliths that mostly consist of olivine, pyroxene, and feldspar (Figure 3a). Mineral fragments include olivine, ringwoodite, pyroxene, and Fe-Ni metal and troilite. Fe-Ni metal and troilite fragments are widespread in the shock vein and occur as spherules with a diameter of 10–30  $\mu\text{m}$  (Figure 3b). The matrix consists of fine-grained mineral clasts less than 10  $\mu\text{m}$ . Maskelynite occurs in the chondritic portions that are adjacent to the shock vein. A few grains in the shock veins also consist of maskelynite. The chemical composition of maskelynite displays a Na-rich content (5.91 wt %) and the anorthite component (An) is 17 mol % (Table 1). The chondritic portion mainly consists of olivine (~40 vol %), pyroxene (~35 vol %), feldspar (~5 vol %), and Fe-Ni metal and troilite (~20 vol %), which are the same as the mineral composition in the shock vein.

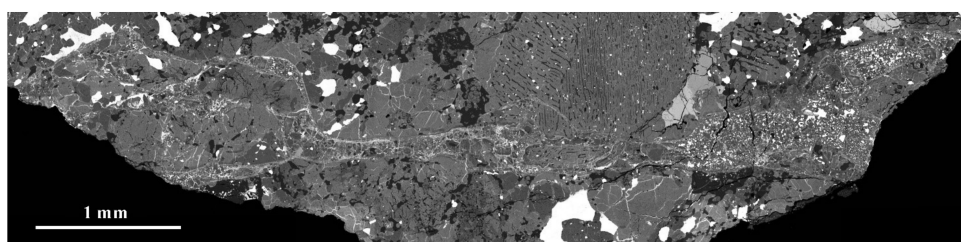


**Figure 2.** Backscattered electron (BSE) image of the shock vein in the GRV053584. The shock vein is located along the sample boundary.

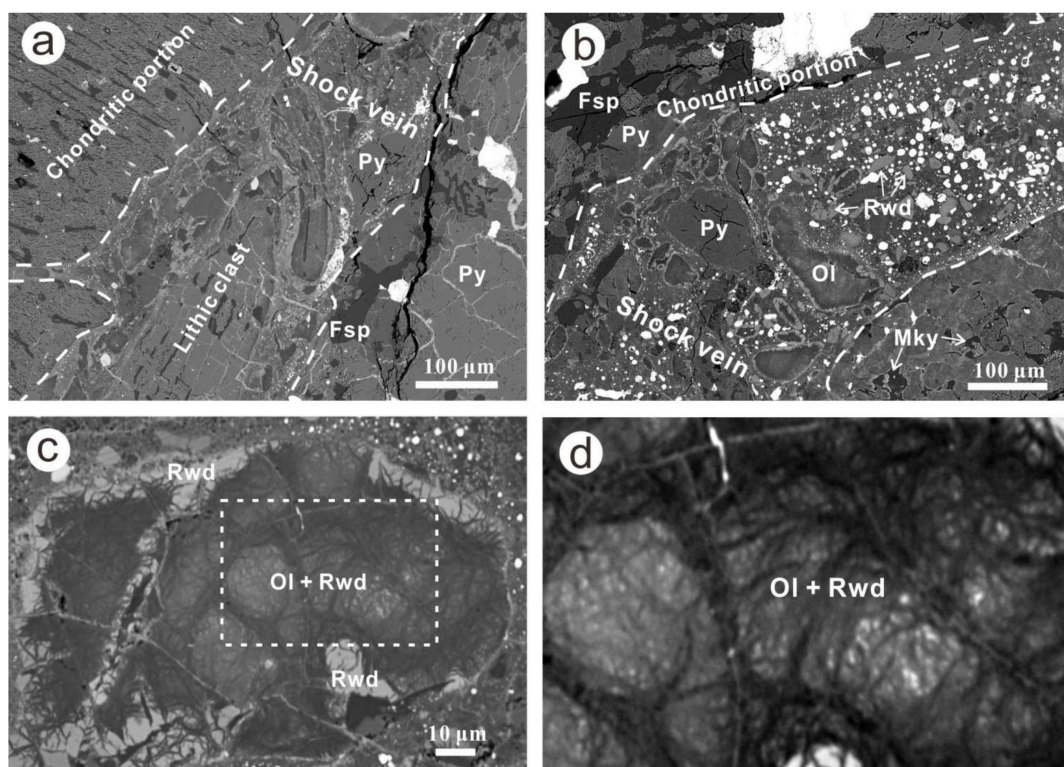


**Figure 3.** (a) Two lithic clasts in the shock vein. The chondritic portion mainly consists of olivine, pyroxene, feldspar, Fe-Ni metal, and troilite. (b) Shocked olivine clasts in the shock vein generally have a ringwoodite rim. The white spherules in the shock vein are Fe-Ni metal and troilite. Note the maskelynite grain adjacent to the shock vein. (c) An olivine-ringwoodite clast with ringwoodite rim and olivine core. (d) High magnification image of the (c). The central region of the clast has a complex structure that consists of olivine and ringwoodite. Fsp—feldspar, Py—pyroxene, Ol—olivine, Mky—maskelynite, Rwd—ringwoodite.

**Table 1.** Representative electron microprobe analyses of olivine-ringwoodite fragments and maskelynite in the shock vein and host olivine grains in the chondritic portion.

Oxide	Ol-Rwd Fragment 1		Ol-Rwd Fragment 2		Host Olivine	Maskelynite
	Rim	Core	Rim	Core		
SiO <sub>2</sub>	37.53	40.87	35.83	41.15	39.09	67.71
TiO <sub>2</sub>	0.01	0.00	0.01	0.00	0.00	-
Al <sub>2</sub> O <sub>3</sub>	0.47	0.00	0.05	0.01	0.00	22.73
FeO	32.49	10.35	36.65	10.29	20.60	1.23
MgO	30.18	48.69	27.01	48.32	40.11	0.23
MnO	0.06	0.39	0.01	0.17	0.47	0.05
CaO	0.13	0.03	0.00	0.04	0.00	2.34
NiO	0.07	0.17	0.01	0.00	0.04	-
Na <sub>2</sub> O	-	-	-	-	-	5.91
K <sub>2</sub> O	-	-	-	-	-	0.44
Total	100.94	100.49	99.56	99.97	100.30	100.64
Fa (mol %)	38	11	43	11	22	An = 17

### 3.2. Shocked Olivine-Ringwoodite and Ringwoodite Clasts

More than 50% clasts in the shock vein are olivine. These olivine clasts occur as coarse-grained polycrystalline aggregates with a diameter of 10–200 μm. Large olivine clasts generally show local

phase transformation along the rims of the grains (Figure 3b,c). The rims are a layer of polycrystalline ringwoodite, with thicknesses ranging from several micrometers to 10  $\mu\text{m}$ . The central region of such clasts mainly consists of olivine. Olivine and ringwoodite are easily distinguished by their different gray level in BSE image, i.e., ringwoodite is brighter than olivine. The olivine core shows a complex structure, with abundant cracks and irregular fractures, organized into a dense network (Figure 3d). However, Raman spectroscopy shows that there is a small amount of ringwoodite in this area. Figure 4 shows two typical Raman spectra of the core. One spectrum displays several peaks at 825, 855, 920, and 961  $\text{cm}^{-1}$ , which is the same as the spectrum of the host olivine. In contrast, another spectrum displays several peaks at 294, 794, 825, 845, 854, and 919  $\text{cm}^{-1}$ , in which the bands at 294, 794, and 845  $\text{cm}^{-1}$  can be assigned to ringwoodite. Electron microprobe analyses reveal that the core contains higher MgO (48.32 wt % and 48.69 wt %) contents and lower FeO (10.29 wt % and 10.35 wt %) contents than the olivine (MgO 40.11 wt % and FeO 20.6 wt %) in the host rock (Table 1). Both Raman spectra and electron microprobe of this area show coexisting olivine and ringwoodite.

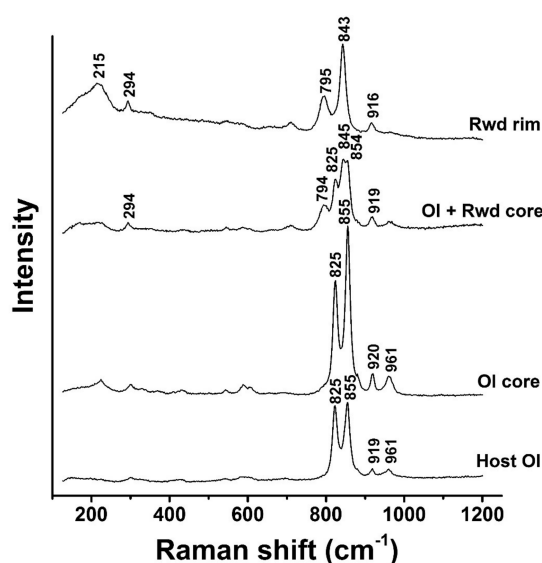


**Figure 4.** Raman spectra of olivine and ringwoodite in the GRV053584. Host Ol—the host olivine clast in the chondritic portion, Ol core and Ol + Rwd core—the central region of the olivine-ringwoodite clast, Rwd rim—the rim region of the olivine-ringwoodite clast.

Ringwoodite occur as individual grains with rounded shape and grain size less than 20  $\mu\text{m}$ . The mean diameter of ringwoodite grains is apparently smaller than that of olivine-ringwoodite grains. And the small clasts (<10  $\mu\text{m}$ ) within the shock vein are completely transformed into ringwoodite. Raman spectrum of the rim contains two strong bands at 795 and 843  $\text{cm}^{-1}$ , which confirms that the rim has the structure of ringwoodite (Figure 4).

An electron microprobe analyses transect collected from one olivine-ringwoodite grain confirms the ringwoodite rim's enrichment in a fayalite (Fa) component compared to the olivine core (Table 2, Figure 5a,b). The maximum Fa component is 42 mol % and the minimum Fa component is 15 mol %. The maximum compositional gap between olivine and ringwoodite is 27 mol %. Electron microprobe X-ray maps of selected elements also appear to show different compositions of magnesium (Mg) and iron (Fe) between olivine core and ringwoodite rim (Figure 5c,d). The Fe and Mg distribution shows a good negative correlation. Fe decreases strongly from the rim to the core, whereas Mg increases from the rim to the core.

**Table 2.** Electron microprobe analyses transect of an olivine-ringwoodite clast.

Oxide	1	2	3	4	5	6	7	8	9	10
SiO <sub>2</sub>	36.72	40.10	39.53	39.23	39.46	39.86	39.59	38.75	38.33	39.76
TiO <sub>2</sub>	0.03	0.00	0.00	0.00	0.00	0.00	0.00	0.00	0.00	0.03
Al <sub>2</sub> O <sub>3</sub>	0.39	0.00	0.00	0.00	0.00	0.00	0.00	0.00	0.01	1.47
FeO	35.43	14.09	18.09	18.60	18.24	15.11	17.35	22.26	24.88	28.03
MgO	27.76	45.57	42.41	41.87	42.19	45.09	43.29	39.49	37.16	26.49
MnO	0.14	0.46	0.47	0.50	0.48	0.48	0.44	0.41	0.37	0.52
NiO	0.22	0.00	0.00	0.01	0.00	0.00	0.00	0.00	0.00	1.19
CaO	0.10	0.02	0.02	0.02	0.03	0.01	0.04	0.02	0.03	0.64
Total	100.78	100.24	100.51	100.23	100.40	100.54	100.72	100.93	100.78	98.13
Fa (mol %)	42	15	19	20	20	16	18	24	27	37

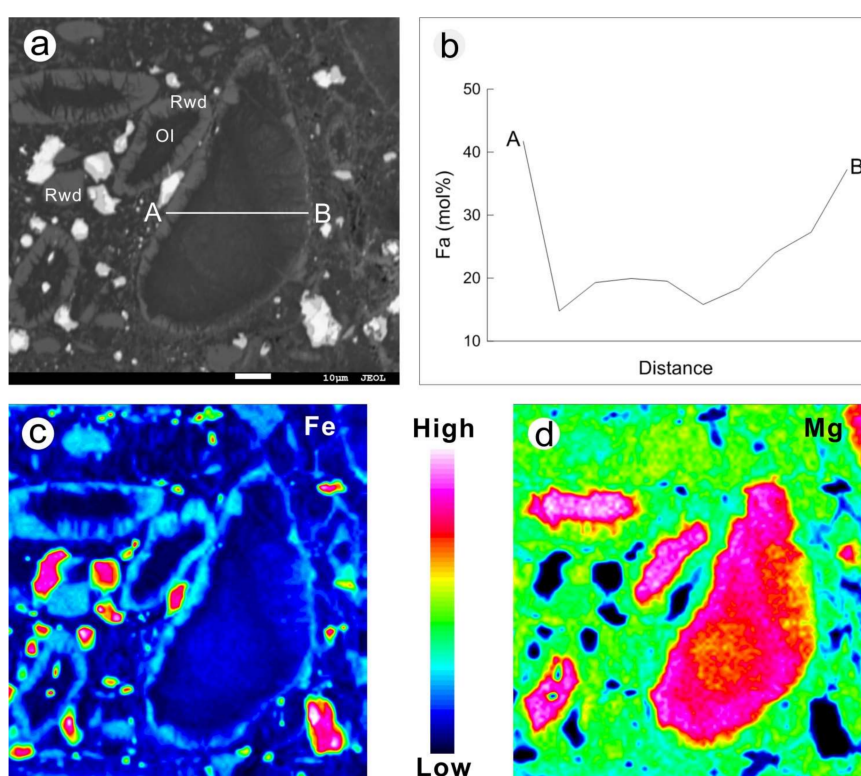


**Figure 5.** (a) A BSE image of four olivine-ringwoodite clasts with a rim of ringwoodite and a core of olivine + ringwoodite. (b) Fa content profile of an olivine-ringwoodite clast. The location measured A-B profile is shown in (a). (c,d) Electron microprobe X-ray elemental maps of iron (Fe) and magnesium (Mg), respectively. Rwd—ringwoodite, Ol—olivine.

## 4. Discussion

### 4.1. Shock Pressure and Temperature of the Shock Vein

High-pressure phases in meteorites can be used to constrain shock pressures. However, due to the interfaces between different minerals and the fractures in meteorites, shock waves could refract and collide in these places, producing localized (micrometer-scale) peak pressures [1]. Therefore, high-pressure phases within and adjacent to shock veins can only represent shock pressures in these places. The most widely used calibration is firstly established by Stöffler et al. [11], then it is revised by Stöffler and Grieve [10] and Fritz et al. [3].

In this study, we try to use the maskelynite to constrain the shock pressure. However, the formation mechanism of maskelynite is still a matter of debate. Many researchers hold that maskelynite is a diaplectic plagioclase glass formed via solid-state transformation [3,40–43]. However, Chen et al. [44] and El Goresy et al. [45] suggested that maskelynite could be formed by melting of plagioclase and is a dense quenched glass. Evidence from Chen et al.'s [44] research include: (1) maskelynite does not display inherited fractures, cleavage and shock-induced deformation features; (2) the grains are smooth and display radiating expansion cracks in neighboring pyroxene. The maskelynite in GRV053584 does not show these melting features. Therefore, the maskelynite in our study is a diaplectic plagioclase glass.

According to the latest shock classifications of meteorites by Fritz et al. [3], the occurrence of maskelynite and ringwoodite in local melt zones of meteorites needs a shock pressure >15 GPa. But this shock classification can't provide the precision formation pressure of maskelynite. Shock experiments by Fritz et al. [46] indicated the shock pressures required for maskelynite decrease with increasing anorthite content, and Ca-rich ( $An_{94}$ ) plagioclase starts transforming into maskelynite at shock pressures ~20 GPa, in contrast to ~30 GPa for albite. Furthermore, research by Gibbons and Ahrens [47] revealed that labradorite ( $An_{63}$ ) almost completely transformed into diaplectic glass under shock pressure of 30–40 GPa. A recent study on maskelynite in asteroidal, lunar and planetary basaltic meteorites shows that maskelynite is a diaplectic glass that forms from plagioclase at shock pressures of ~20–30 GPa, depending on the Ca concentration [40]. Hence, we can conclude that plagioclase starts transforming into maskelynite at ~20–30 GPa and completely transforms into maskelynite at ~40 GPa. Lingunite (hollandite-type  $NaAlSi_3O_8$ ) is a high-pressure polymorph of plagioclase [48,49]. Gillet et al. [48] identified lingunite in shock-induced melt veins of the Sixiangkou L6 chondrite and found that it is intergrown with feldspatic glass within maskelynite. They suggested the shock pressures and the shock temperatures for the transformation of plagioclase into lingunite are 21–23 GPa and 2273–2373 K, respectively. Similarly, the shock pressure necessary for the plagioclase-lingunite transformation is also correlated with original composition of plagioclase [49,50].

In our study on GRV053584, we did not find that lingunite and the maskelynite is a diaplectic plagioclase glass. Based on its anorthite component ( $An_{17}$ ), we estimated the peak shock pressure in the shock vein of GRV053584 is ~30 GPa (Figure 6) [40,46]. Nevertheless, two studies of L6 chondrite Asuka 09584 [23] and L5 chondrite Dhofar 1970 [51] indicated that the formation of ringwoodite rims around olivine cores needs shock pressures of <24 GPa and 20–25 GPa, respectively. Therefore, the shock pressure in GRV053584 exceeds the forming pressure of the ringwoodite rim. Exceeding pressure is good for the olivine-ringwoodite transformation process. This is because the formation of high pressure phases requires an excess of pressure to activate nucleation [1].

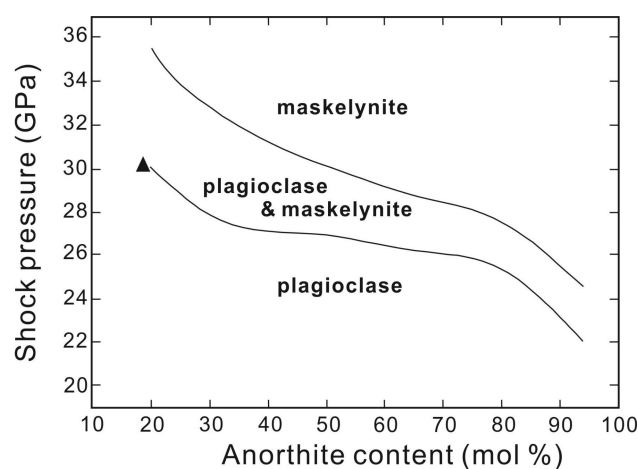


**Figure 6.** Pressure-composition phase diagram for shocked plagioclase (Filled triangle represents this study). Modified after Fritz et al. [46].

#### 4.2. Olivine-Ringwoodite Transformation Process

The olivine-ringwoodite transformation is a reconstructive process that involves breaking of chemical bonds in olivine and rearrangements of cations and anion sublattices in ringwoodite [25]. The phase transformation from olivine to ringwoodite can take place in the following ways: incoherent grain-boundary nucleation and interface-controlled growth [34,52], incoherent intracrystalline growth [38], coherent intracrystalline growth [37], coherent intracrystalline martensitic transformation [35,36], combination of coherent and incoherent growth [39], crystallizing from olivine melts [7].

In this study, the formation of the ringwoodite rims is consistent with the mechanism of solid-state incoherent grain-boundary transformation. The following two evidences support this hypothesis. First, ringwoodite mainly appears in the rim of a clast. Although there are a few small individual ringwoodite grains in the shock vein, they might be the edges of larger olivine-ringwoodite clasts and only ringwoodite rims have been exposed by sample cutting and polishing. The occurrence of ringwoodite rims around olivine cores indicates that ringwoodite preferentially take place on grain boundaries. Chen et al. [25] proposed that since nucleation of crystals tends to occur at grain boundaries, edges, corners, and shear planes, it appears that the phase transformation of olivine to high-pressure polymorphs may preferentially take place on grain boundaries and planar defects including fractures and stacking faults. Second, ringwoodite rims are polycrystalline aggregates. Polycrystalline ringwoodite is a feature of incoherent growth mechanism [2]. Ringwoodite rims around olivine cores are also reported in Antarctic chondrite GRV 022321 [53], Asuka 09584 [23], and Dhofar 1970 [51]. The occurrences of ringwoodite rims in these meteorites are unexceptionally interpreted as a result of solid-transformation from olivine.

Shock veins in meteorites are the results of shear faulting and frictional melting under differential stress [11]. Minerals in the shock veins have been definitely affected by high pressure and high temperature. Maskelynite adjacent to the shock vein of GRV053584 indicates a peak shock pressure ~30 GPa. Shock-induced high pressure can reach pressure equilibrium about a microsecond in a typical chondrite with millimeter-sized grains [1], whereas shock-induced high temperature could not be homogenous in that time. A single olivine grain in the shock vein of GRV053584 has undoubtedly undergone the same shock pressure. The difference of shock conditions between the rim and the core is only temperature. The rims of the original olivines are close to shock melt vein matrix and are heated to a high temperature [39]. Therefore, high temperature plays a key role in the olivine-ringwoodite transformation. Olivine-ringwoodite grains in the shock vein of GRV053584 with rounded shape imply they are heated to high temperature. In addition to this, the smooth and round outlines of Fe-Ni and FeS spherules indicate a total melting of Fe-Ni metal and troilite and imply a shock temperature more than 850 °C [54]. For the olivine-ringwoodite clasts, the surface layer of ringwoodite which is close to the melt matrix is denser than the core ringwoodite. This indicates the transformation begin from the rims of the clasts. This hypothesis can be supported by the investigations of ringwoodite lamellae in olivine in the shock veins of Sixiangkou chondrite [31] and Yamato 791384 chondrite [39]. Chen et al. [31] reported that ringwoodite lamellae in the rim of olivine grains are thicker and have higher densities than in their interior.

Electron microprobe analyses of olivine-ringwoodite grains show different amount of Mg and Fe, where ringwoodite are richer in Fe and poorer in Mg. The higher Fa content in the ringwoodite rims in compassion with a lower Fa content in the olivine cores supports compositional diffusion of Fe during nucleation and growth of ringwoodite rim. Mg-Fe diffusion is a common phenomenon in the transformation process of olivine-ringwoodite, whether the intracrystalline transformation mechanism or the interface-controlled mechanism. This is because, during the nucleation and growth of ringwoodite, iron was preferentially partitioned to ringwoodite with magnesium partitioning in olivine [51]. Katsura and Ito's [55] experimental work also supported this hypothesis. They demonstrated that during a diffusion-controlled solid-state phase transformation, iron is partitioned into the  $\beta$ -olivine and  $\gamma$ -olivine structure, leading to iron-rich wadsleyite and ringwoodite and Fe-poor olivine. As the ringwoodite rim

has a higher Fa content, the transformation was likely controlled by diffusion under shock-induced high-temperature conditions [1,43].

## 5. Conclusions

The GRV053584 chondrite underwent strong shock events. Olivine clasts in the melt vein generally display shock feature of irregular fractures and phase transformation (ringwoodite rim around olivine core). The Na-rich maskelynite adjacent to the shock vein indicates a shock pressure of ~30 GPa. The FeO content at the ringwoodite rim is higher than in the olivine core and the component diffusion indicates the transformation process of olivine to ringwoodite is a diffusion-controlled incoherent nucleation and growth. The spatial association between ringwoodite and the shock melt vein matrix suggests that high temperature plays a key role in prompting phase transformation.

**Acknowledgments:** This work was jointly funded by the National Natural Science Foundation of China (41503062, 41702129, and 41673070), and Natural Science Foundation of Hunan Province (2016JJ6039). We thank Changming Xing for helping with the EPMA analysis. Three anonymous reviewers are thanked for their constructive comments and suggestions which greatly improved the quality of this paper.

**Author Contributions:** Feng Yin and Zhiwei Liao conceived and designed the experiments; Feng Yin performed the experiments; Feng Yin, Zhiwei Liao and Deqiu Dai analyzed the data; Feng Yin wrote the paper, assisted by all other authors; and Andrew Hursthouse and Zhiwei Liao contributed to the revising of the paper.

**Conflicts of Interest:** The authors declare no conflict of interest.

## References

1. Sharp, T.G.; DeCarli, P.S. Shock effects in meteorites. In *Meteorites and the Early Solar System II*; Lauretta, D.S., McSween, H.Y., Jr., Eds.; University of Arizona Press: Tucson, AZ, USA, 2006; pp. 653–677.
2. Tomioka, N.; Miyahara, M. High-pressure minerals in shocked meteorites. *Meteorit. Planet. Sci.* **2017**, *52*, 2017–2039. [[CrossRef](#)]
3. Fritz, J.; Greshake, A.; Fernandes, V.A. Revising the shock classification of meteorites. *Meteorit. Planet. Sci.* **2017**, *52*, 1216–1232. [[CrossRef](#)]
4. Clark, S.P.; Ringwood, A. Density distribution and constitution of the mantle. *Rev. Geophys.* **1964**, *2*, 35–88. [[CrossRef](#)]
5. Ringwood, A. A model for the upper mantle. *J. Geophys. Res.* **1962**, *67*, 857–867. [[CrossRef](#)]
6. Walton, E.L. Shock metamorphism of Elephant Moraine A79001: Implications for olivine–ringwoodite transformation and the complex thermal history of heavily shocked Martian meteorites. *Geochim. Cosmochim. Acta* **2013**, *107*, 299–315. [[CrossRef](#)]
7. Miyahara, M.; El Goresy, A.; Ohtani, E.; Nagase, T.; Nishijima, M.; Vashaei, Z.; Ferroir, T.; Gillet, P.; Dubrovinsky, L.; Simionovici, A. Evidence for fractional crystallization of wadsleyite and ringwoodite from olivine melts in chondrules entrained in shock-melt veins. *Proc. Natl. Acad. Sci. USA* **2008**, *105*, 8542–8547. [[CrossRef](#)] [[PubMed](#)]
8. Greshake, A.; Fritz, J.; Böttger, U.; Goran, D. Shear-induced ringwoodite formation in the Martian shergottite Dar al Gani 670. *Earth Planet. Sci. Lett.* **2013**, *375*, 383–394. [[CrossRef](#)]
9. Ma, C.; Tschauer, O.; Beckett, J.R.; Liu, Y.; Rossman, G.R.; Sinogeikin, S.V.; Smith, J.S.; Taylor, L.A. Ahrensite,  $\gamma$ -Fe<sub>2</sub>SiO<sub>4</sub>, a new shock-metamorphic mineral from the Tissint meteorite: Implications for the Tissint shock event on Mars. *Geochim. Cosmochim. Acta* **2016**, *184*, 240–256. [[CrossRef](#)]
10. Stöffler, D.; Grieve, R. Impactites. In *Metamorphic Rocks: A Classification and Glossary of Terms, Recommendations of the International Union of Geological Sciences*; Fettes, D., Desmons, J., Eds.; Cambridge University Press: Cambridge, UK, 2007; pp. 82–92, 111–125, 126–242.
11. Stöffler, D.; Keil, K.; Scott, E.R.D. Shock metamorphism of ordinary chondrites. *Geochim. Cosmochim. Acta* **1991**, *55*, 3845–3867. [[CrossRef](#)]
12. Agee, C.B. Phase transformations and seismic structure in the upper mantle and transition zone. *Rev. Mineral. Geochem.* **1998**, *37*, 165–203.
13. Stein, S.; Rubie, D.C. Deep earthquakes in real slabs. *Science* **1999**, *286*, 909–910. [[CrossRef](#)]

14. Rubie, D.C.; Ross, C.R. Kinetics of the olivine-spinel transformation in subducting lithosphere: Experimental constraints and implications for deep slab processes. *Phys. Earth Planet. Int.* **1994**, *86*, 223–243. [[CrossRef](#)]
15. Tschauner, O.; Ma, C.; Beckett, J.R.; Prescher, C.; Prakapenka, V.B.; Rossman, G.R. Discovery of bridgmanite, the most abundant mineral in Earth, in a shocked meteorite. *Science* **2014**, *346*, 1100–1102. [[CrossRef](#)] [[PubMed](#)]
16. Ohtani, E.; Suzuki, A.; Kato, T. Flotation of olivine and diamond in mantle melt at high pressure: Implications for fractionation in the deep mantle and ultradeep origin of diamond. In *Properties of Earth and Planetary Materials at High Pressure and Temperature*; Geophysical Monograph Series; Manghnani, M.H., Yagi, T., Eds.; AGU: Washington, DC, USA, 1998; pp. 227–239.
17. Ito, E.; Takahashi, E. Postspinel transformations in the system  $Mg_2SiO_4$ - $Fe_2SiO_4$  and some geophysical implications. *J. Geophys. Res.* **1989**, *94*, 10637–10646. [[CrossRef](#)]
18. Ohtani, E. Melting relation of  $Fe_2SiO_4$  up to about 200 kbar. *J. Phys. Earth* **1979**, *27*, 189–208. [[CrossRef](#)]
19. Li, C.M.; Bassett, W.A. The postspinel phases in the  $Mg_2SiO_4$ - $Fe_2SiO_4$  system. *Science* **1975**, *187*, 66–68.
20. Kumazawa, M.; Sawamoto, H.; Ohtani, E.; Masaki, K. Postspinel phase of forsterite and evolution of the Earth's mantle. *Nature* **1974**, *247*, 356–358. [[CrossRef](#)]
21. Binns, R.A.; Davis, R.J.; Reed, S.J.B. Ringwoodite, natural  $(Mg,Fe)_2SiO_4$  spinel in the Tenham meteorite. *Nature* **1969**, *221*, 943–944. [[CrossRef](#)]
22. Miyahara, M.; Ohtani, E.; El Goresy, A.; Ozawa, S.; Gillet, P. Phase transition processes of olivine in the shocked Martian meteorite Tissint: Clues to origin of ringwoodite-, bridgmanite- and magnesiowüstite-bearing assemblages. *Phys. Earth Planet. Int.* **2016**, *259*, 18–28. [[CrossRef](#)]
23. Pittarello, L.; Ji, G.; Yamaguchi, A.; Schryvers, D.; Debaille, V.; Claeys, P. From olivine to ringwoodite: A TEM study of a complex process. *Meteorit. Planet. Sci.* **2015**, *50*, 944–957. [[CrossRef](#)]
24. Xie, Z.; Sharp, T.G. Host rock solid-state transformation in a shock-induced melt vein of Tenham L6 chondrite. *Earth Planet. Sci. Lett.* **2007**, *254*, 433–445. [[CrossRef](#)]
25. Chen, M.; Li, H.; El Goresy, A.; Liu, J.; Xie, X. Fracture-related intracrystalline transformation of olivine to ringwoodite in the shocked Sixiangkou meteorite. *Meteorit. Planet. Sci.* **2006**, *41*, 731–737. [[CrossRef](#)]
26. Beck, P.; Gillet, P.; El Goresy, A.; Mostefaoui, S. Timescales of shock processes in chondritic and martian meteorites. *Nature* **2005**, *435*, 1071–1074. [[CrossRef](#)] [[PubMed](#)]
27. Sharp, T.G.; Xie, Z.; DeCarli, P.S.; Hu, J. A large shock vein in L chondrite Roosevelt County 106: Evidence for a long-duration shock pulse on the L chondrite parent body. *Meteorit. Planet. Sci.* **2015**, *50*, 1941–1953. [[CrossRef](#)]
28. Feng, L.; Lin, Y.; Hu, S.; Xu, L.; Miao, B. Estimating compositions of natural ringwoodite in the heavily shocked Grove Mountains 052049 meteorite from Raman spectra. *Am. Mineral.* **2011**, *96*, 1480–1489. [[CrossRef](#)]
29. Pearson, D.G.; Brenker, F.E.; Nestola, F.; McNeill, J.; Nasdala, L.; Hutchison, M.T.; Matveev, S.; Mather, K.; Silversmit, G.; Schmitz, S.; et al. Hydrous mantle transition zone indicated by ringwoodite included within diamond. *Nature* **2014**, *507*, 221–224. [[CrossRef](#)] [[PubMed](#)]
30. Chen, M.; Sharp, T.G.; El Goresy, A.; Wopenka, B.; Xie, X. The majorite-pyrope + magnesiowüstite assemblage: Constraints on the history of shock veins in chondrites. *Science* **1996**, *271*, 1570–1573. [[CrossRef](#)]
31. Chen, M.; El Goresy, A.; Gillet, P. Ringwoodite lamellae in olivine: Clues to olivine-ringwoodite phase transition mechanisms in shocked meteorites and subducting slabs. *Proc. Natl. Acad. Sci. USA* **2004**, *101*, 15033–15037. [[CrossRef](#)] [[PubMed](#)]
32. Vaughan, P.J.; Green, H.W.; Coe, R.S. Is the olivine-spinel phase transformation martensitic? *Nature* **1982**, *298*, 357–358. [[CrossRef](#)]
33. Sung, C.; Burns, R.G. Kinetics of the olivine→spinel transition: Implications to deep-focus earthquake genesis. *Earth Planet. Sci. Lett.* **1976**, *32*, 165–170. [[CrossRef](#)]
34. Mosenfelder, J.L.; Marton, F.C.; Ross, C.R., II; Kerschhofer, L.; Rubie, D.C. Experimental constraints on the depth of olivine metastability in subducting lithosphere. *Phys. Earth Planet. Int.* **2001**, *127*, 165–180. [[CrossRef](#)]
35. Burnley, P.C.; Green, H.W. Stress dependence of the mechanism of the olivine-spinel transformation. *Nature* **1989**, *338*, 753–756. [[CrossRef](#)]
36. Boland, J.N.; Liu, L. Olivine to spinel transformation in  $Mg_2SiO_4$  via faulted structures. *Nature* **1983**, *303*, 233–235. [[CrossRef](#)]
37. Kerschhofer, L.; Sharp, T.G.; Rubie, D.C. Intracrystalline transformation of olivine to wadsleyite and ringwoodite under subduction zone conditions. *Science* **1996**, *274*, 79–81. [[CrossRef](#)]

38. Chen, M.; Chen, J.; Xie, X.; Xu, J. A microstructural investigation of natural lamellar ringwoodite in olivine of the shocked Sixiangkou chondrite. *Earth Planet. Sci. Lett.* **2007**, *264*, 277–283. [[CrossRef](#)]
39. Miyahara, M.; Ohtani, E.; Kimura, M.; El Goresy, A.; Ozawa, S.; Nagase, T.; Nishijima, M.; Hiraga, K. Coherent and subsequent incoherent ringwoodite growth in olivine of shocked L6 chondrites. *Earth Planet. Sci. Lett.* **2010**, *295*, 321–327. [[CrossRef](#)]
40. Rubin, A.E. Maskelynite in asteroidal, lunar and planetary basaltic meteorites: An indicator of shock pressure during impact ejection from their parent bodies. *Icarus* **2015**, *257*, 221–229. [[CrossRef](#)]
41. Jaret, S.J.; William, R.W.; Brian, L.P.; Lars, E.; Hanna, N.; Shawn, P.W.; Timothy, D.G. Maskelynite formation via solid-state transformation: Evidence of infrared and X-ray anisotropy. *J. Geophys. Res. Planet* **2015**, *120*, 570–587. [[CrossRef](#)]
42. Bunch, T.E.; Cohen, A.J.; Dence, M.R. Natural terrestrial maskelynite. *Am. Mineral.* **1967**, *52*, 244–253.
43. Stöffler, D. Maskelynite confirmed as diaplectic glass: Indication for peak shock pressures below 45 GPa in all Martian meteorites. In Proceedings of the 31st Annual Lunar and Planetary Science Conference, Houston, TX, USA, 13–17 March 2000.
44. Chen, M.; El Goresy, A. The nature of maskelynite in shocked meteorites: Not diaplectic glass but a glass quenched from shock-induced dense melt at high pressures. *Earth Planet. Sci. Lett.* **2000**, *179*, 489–502. [[CrossRef](#)]
45. El Goresy, A.; Gillet, P.; Miyahara, M.; Ohtani, E.; Ozawa, S.; Beck, P.; Montagnac, G. Shock-induced deformation of Shergottites: Shock-pressures and perturbations of magmatic ages on Mars. *Geochim. Cosmochim. Acta* **2013**, *101*, 233–262. [[CrossRef](#)]
46. Fritz, J.; Wünnemann, K.; Greshake, A.; Fernandes, V.A.S.M.; Boettger, U.; Hornemann, U. Shock pressure calibration for Lunar plagioclase. In Proceedings of the 42nd Lunar and Planetary Science Conference, Woodlands, TX, USA, 7–11 March 2011.
47. Gibbons, R.V.; Ahrens, T.J. Effects of shock pressures on calcic plagioclase. *Phys. Chem. Miner.* **1977**, *1*, 95–107. [[CrossRef](#)]
48. Gillet, P.; Chen, M.; Dubrovinsky, L.; El Goresy, A. Natural NaAlSi<sub>3</sub>O<sub>8</sub>-Hollandite in the Shocked Sixiangkou Meteorite. *Science* **2000**, *287*, 1633–1636. [[CrossRef](#)] [[PubMed](#)]
49. Liu, L.G.; El Gorsey, A. High-pressure phase transitions of the feldspars, and further characterization of lingunite. *Int. Geol. Rew.* **2007**, *49*, 854–860. [[CrossRef](#)]
50. Liu, L. High-pressure phase transformations of albite, jadeite and nepheline. *Earth Planet. Sci. Lett.* **1978**, *37*, 438–444. [[CrossRef](#)]
51. Walton, E.L.; McCarthy, S. Mechanisms of ringwoodite formation in shocked meteorites: Evidence from L5 chondrite Dhofar 1970. *Meteorit. Planet. Sci.* **2017**, *52*, 762–776. [[CrossRef](#)]
52. Liu, M.; Kerschhofer, L.; Mosenfeldaenr, J.L.; Rubie, D.C. The effect of strain energy on growth rates during the olivine-spinel transformation and implications for olivine metastability in subducting slabs. *J. Geophys. Res. Sol.* **1998**, *103*, 23897–23909. [[CrossRef](#)]
53. Xie, Z.; Sharp, T.G.; DeCarli, P.S. Ringwoodite rims around olivine cores in shock-induced melt veins of an antarctic chondrite: Mechanisms of transformation and Fe-Mg diffusion. In Proceedings of the 73rd Annual Meteoritical Society Meeting, New York, NY, USA, 26–30 July 2010.
54. Tomkins, A.G. What metal-troilite textures can tell us about post-impact metamorphism in chondrite meteorites. *Meteorit. Planet. Sci.* **2009**, *44*, 1133–1149. [[CrossRef](#)]
55. Katsura, T.; Ito, E. The system Mg<sub>2</sub>SiO<sub>4</sub>-Fe<sub>2</sub>SiO<sub>4</sub> at high pressures and temperatures: Precise determination of stabilities of olivine, modified spinel, and spinel. *J. Geophys. Res.* **1989**, *94*, 15663–15670. [[CrossRef](#)]

